Available online at www.sciencedirect.com
ScienceDirect
International Journal of Heat and Mass Transfer 49 (2006) 4921–4931
International Journal of HEAT and MASS TRANSFER
www.elsevier.com/locate/ijhmt

A molecular dynamics study of interfacial thermal transport in heterogeneous systems

Phil J. Hegedus, Alexis R. Abramson *

Department of Mechanical and Aerospace Engineering, Case Western Reserve University, 610 Glennan Building, 10900 Euclid Avenue, Cleveland, OH 44106, United States

Received 2 November 2005; received in revised form 24 May 2006
Available online 22 August 2006

Abstract

Non-equilibrium molecular dynamics software was developed to study thermal transport at the nanoscale. Lennard–Jones parameters of pure argon (mass and bond strength) were systematically modified to create heterogeneous thin film systems, including layered systems and nanocomposites, to investigate the influence of interfaces on thermal conductivity. Results were analyzed using combinations of kinetic theory and a thermal resistance network model together with the acoustic mismatch model (AMM). The introduction of a second material into an argon film generally decreased its overall thermal conductivity. Moreover, the presence of a nanoparticle was less influential in reducing thermal conductivity than the addition of a thin layer.

Keywords: Molecular dynamics; Interfacial thermal resistance; Nanoparticle

1. Introduction

The ever-increasing demand for faster integrated circuits, larger data storage capacity, and better medical diagnostic and treatment capabilities has jumpstarted the field of nanoscience. Moreover, modern silicon microelectronics are now firmly in the nanoscale regime (<100 nm). As devices approach the nanoscale, many standard tools for solving engineering problems reach a limit of applicability because of failures in the assumptions from which those tools are built. Thermal management is one of the most frequently encountered problems at this design level, yet processes such as refrigeration, cooling and power generation would benefit largely from advances in thermal efficiency and thermal management. However, a complete picture illustrating the mechanisms that influence nanoscale thermal transport has not yet taken form. Heat flow can be inhibited or enhanced by a number of phenomena including but not limited to interstitial atoms, vacancies, pores, single atom or multi-atom (nanoparticles) impurities, lattice strain, interfaces, edge and screw dislocations, and grain boundaries. The extent to which each of these phenomena plays a role in influencing thermal transport is relatively unknown, thus an analysis of these mechanisms is necessary in order to develop a better understanding of nanoscale heat transfer. In particular, interfacial effects are an example of a mechanism which can be critical at small length scales, and through thorough investigation, its role in the larger picture of nanoscale thermal transport can be made clearer [1].

Previous research has shown that molecular dynamics (MD) is a viable method for providing insight into the nanoscale world, especially where thermal transport is concerned [2–8]. Depending on the size and state of the system, as well as how well the underlying physics are understood, MD can provide the necessary properties, such as thermal conductivity, for use in already existing tools and techniques, or slightly modified ones. More importantly, MD is adjustable and can uncover trends that can lead to a

* Corresponding author. Tel.: +1 216 368 4191; fax: +1 216 368 3007.
E-mail address: alexis.abramson@case.edu (A.R. Abramson).

0017-9310/$ - see front matter © 2006 Elsevier Ltd. All rights reserved.
doi:10.1016/j.ijheatmasstransfer.2006.05.030

Nomenclature

Latin characters

a_0	equilibrium lattice constant
C	heat capacity
g	spring constant of harmonic oscillator
$\hbar$	Planck's constant divided by 2π
k	thermal conductivity
k_B	Boltzmann's constant
$\mathbf{k}$	wavevector
k_{eff}	effective thermal conductivity
ℓ	phonon mean free path (MFP)
m	atomic mass
Q	heat flux
r_c	atomic interaction cut off distance
r_{ij}	separation distance between atoms i and j
r_0	equilibrium separation distance
R_B	interfacial/thermal boundary resistance
T	temperature
x	horizontal simulation cell dimension (width)
y	lateral simulation cell dimension (height)
Z	lateral simulation cell dimension (depth)
Z_i	acoustic impedance of material i

Greek symbols

$\alpha_{i\to j}$	transmission probability of phonons traveling from material i to material j
$\Gamma_{i,j}$	AMM transmission coefficient of material i and mode of propagation j
ΔT	temperature difference
ε	Lennard–Jones well depth parameter
θ	angle of incidence of phonon on interface
Θ_D	Debye temperature
v_i	mean phonon speed of sound of material i
v_s	speed of sound
ρ_i	density of material i
σ	Lennard–Jones length scale parameter
τ	mean time between phonon collisions
Φ_{LJ}	Lennard–Jones potential
ω_D	Debye frequency

better overall understanding of the underlying physics present in special materials. For instance, Lukes et al. [4] investigated nanoporous thin films using non-equilibrium molecular dynamics (NEMD). They found that as the film's porosity increased, the dependence of thermal conductivity on temperature decreased. Moreover, the thermal conductivity became independent of temperature for pores of 5 or more atomic vacancies. Volz et al. [9] investigated the interfacial effects in silicon–germanium superlattices and discovered that strain greatly affects the overall thermal conductivity of the superlattices, all the while showing an improved agreement with experimental values. Abramson et al. [5] used NEMD simulations to study how various factors affect the thermal conductivity of bi-material thin films containing one or more solid–solid interfaces. Results suggested that variation of material composition ratios had little influence on the thermal behavior observed at or near the interfaces and that the inclusion of multiple interfaces within a bi-material film did not produce a proportional decrease in its overall thermal conductivity. In addition, a significant decrease in thermal conductivity due to lattice strain was observed when a coherent interface between two materials of different lattice constants was forced. Stevens et al. [10] utilized NEMD to study the thermal boundary resistance between two FCC structured Lennard–Jones crystals well above the Debye temperature. The study showed a strong temperature dependence of thermal boundary resistance R_B, suggesting that inelastic scattering of phonons at the interface plays a major role in thermal transport.

The most important factor determining the success of a classical MD simulator is its interatomic potential. The Lennard–Jones interatomic potential, also known as the LJ, 12–6, or 6–12 potential, is the best known and the one most commonly used for studying thermal transport. It provides a fairly realistic description of the interaction between two electrically non-conductive elements with filled valence shells. For a pair of atoms i and j the Lennard–Jones potential is:

$$\Phi_{LJ}(r_{ij}) = 4\varepsilon\left[\left(\frac{\sigma}{r_{ij}}\right)^{12} - \left(\frac{\sigma}{r_{ij}}\right)^{6}\right] \tag{1}$$

where r_{ij} is the separation distance between two atoms. The well depth parameter ε defines the strength of interaction between two like atoms at their lowest possible energy state, which corresponds to a separation distance equal to the nearest neighbor distance r_0. The separation parameter σ defines a length scale over which the interaction occurs; it is the distance between two atoms where their relative energy potential is zero. In a heterogeneous Lennard–Jones system with one or more interfaces, interfacial thermal resistance is influenced by the relative values of mass and the Lennard–Jones parameters. This is expected since the interatomic potential plays a large role in determining the thermal conductivity. To illustrate the effect on interatomic potential, Fig. 1 compares the original Lennard–Jones potential for argon to two ε-modified potentials. As ε increases, the well depth increases, effectively making it more difficult for the atoms to travel away from their equilibrium positions. Conversely, as ε decreases, the well depth decreases and the atoms feel less restricted in motion. Since phonons are influenced by atomic motion, it is evident that thermal transport will consequently be affected. It is the intention of this paper to study how variables such as mass and interatomic potential affect interfacial thermal resis-

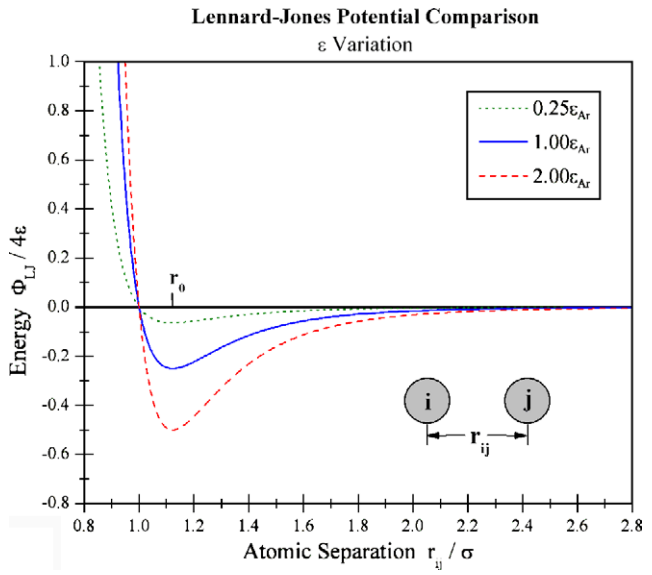

Fig. 1. The Lennard–Jones potential is compared to two cases of ε variation: 0.25ε and 2.00ε. The equilibrium separation distance r_0 is also shown.

tance in heterogeneous systems through the use of molecular dynamics and to compare the results with basic theories on the subject.

1.1. Thermal transport theory

While an MD simulation can provide information about thermal behavior, it is important to examine thermal transport from a theoretical perspective to help interpret those results. Because argon, the base material for all simulations in this study, is a dielectric and no electromagnetic energy is introduced into the system, phonons are responsible for all thermal energy transport. Therefore, kinetic theory (KT) as applied to phonons provides an interesting means for comparison with MD simulation results on the subject of thermal transport. Using KT, the thermal conductivity of a solid can be approximated by the following expression:

$$k = \frac{1}{3} C v \ell \tag{2}$$

where C is the heat capacity, v is the mean phonon speed of sound, and ℓ is the phonon mean free path (MFP). While this equation does not encompass a complete theoretical framework of thermal transport, it is a valuable tool to use for providing insight to the mechanisms that may be influencing the thermal conductivity of heterogeneous systems. Applying kinetic theory to heterogeneous systems is complicated by the fact that each material exhibits different properties, and the use of a simple averaging technique may be considered questionable. Therefore, kinetic theory values for thermal conductivity were compared with MD results on systems of films comprised of only one type of material (e.g. argon). However, because the Lennard–Jones parameters were systematically varied in the simulations, comparison of a kinetic theory analysis to results obtained using "fictitious" materials, or argon-*variants*, with unknown values of C, v and l becomes difficult. Nonetheless, to prepare for an appropriate comparison with the argon variants, various assumptions were made and a new approach was developed described as follows.

At low temperatures, the average kinetic energy of an atom is low enough that its displacement from equilibrium at any given moment is very small. Therefore, the movement can be approximated as a harmonic oscillator. An approximation of atomic velocity based on harmonic oscillation may be given by

$$v_{\mathrm{HO}} \approx r_0 \sqrt{\frac{g}{m}} \tag{3}$$

where g is the material's spring stiffness. The equilibrium spring stiffness can be easily obtained by differentiating the Lennard–Jones potential twice with respect to r_{ij} and evaluating it at the point where potential energy is at a minimum ($r_{ij} = r_0$). By evaluating r_{ij} at the nearest neighbor distance r_0, an expression for a Lennard–Jones harmonic oscillator velocity may be calculated [5]:

$$v_{\mathrm{LJ}} \approx \frac{r_0}{\sigma} \sqrt{\frac{72\varepsilon}{2^{1/3} m}} \tag{4}$$

It should be noted that the Lennard–Jones velocity produced here is not directly related to the phonon speed of sound. Using the appropriate LJ parameters for pure argon, the above velocity is calculated as 1311.9 m/s. The longitudinal and transverse speeds of sound for argon under the same conditions are 1575.0 m/s and 961.7 m/s, respectively [11]. Adjusting for direction of propagation, the average speed of sound in the (100) direction is 1062.0 m/s. Despite this difference, the Lennard–Jones harmonic oscillator velocity from Eq. (3) can arguably be used to estimate the phonon speed of sound, and can be subsequently used in Eq. (2) to help determine thermal conductivity. The Lennard–Jones harmonic oscillator velocities of the new argon variants were calculated from Eq. (4) using the systematically incremented values for m, ε and σ.

An estimation of the phonon mean free path, required in Eq. (2), for argon and its variants was not quite as straightforward. Experimental data [12,13] were used to determine that $\ell \approx 15.0$ Å at $T = 57.3$ K, the steady-state temperature observed in the simulations performed for this study. Employing the harmonic oscillator expression for velocity in Eq. (4) and the relationship $v_{\mathrm{LJ}} = l/\tau$, where τ is the mean free time of argon which is assumed to remain constant, the MFP of each argon *variant* was estimated from pure argon by

$$\frac{\ell^*}{\ell_{\mathrm{Ar}}} = \frac{\sigma_{\mathrm{Ar}}}{\sigma^*} \sqrt{\frac{\varepsilon^* m_{\mathrm{Ar}}}{\varepsilon_{\mathrm{Ar}} m^*}} \tag{5}$$

where terms with subscript Ar refer to values for pure argon and terms with superscript $*$ refer to the Lennard–Jones variations of argon.

The final parameter examined with respect to the kinetic theory approximation in Eq. (2) is heat capacity. Using the Debye approximation, the heat capacity of any material can be written in terms of the Debye temperature, Θ_D, as [14]:

$$C = \frac{3k_B^4}{2\pi^2}\left(\frac{T}{\hbar v_s}\right)^3 \int_{x=0}^{\Theta_D/T} \frac{x^4 e^x}{(e^x-1)^2}\,dx \tag{6}$$

where T is the average lattice temperature and $x = \hbar v_s \mathbf{k}/k_B T$, where $\mathbf{k}$ is a phonon wavevector. The Debye temperature is given by [14]

$$k_B \Theta_D = \hbar v \mathbf{k}_D \tag{7}$$

where k_B is Boltzmann's constant, $\hbar$ is Planck's constant divided by 2π and $\mathbf{k}_D$ is the Debye cutoff wavevector. Therefore, in a manner similar to the calculation of the MFP for the variants, the new materials' Debye temperatures were determined as a function of Lennard–Jones parameters:

$$\frac{\Theta_D^*}{\Theta_{D,Ar}} = \frac{\sigma_{Ar}}{\sigma^*}\sqrt{\frac{\varepsilon^*}{\varepsilon_{Ar}}\frac{m_{Ar}}{m^*}} \tag{8}$$

which then allows for approximation of C. For Lennard–Jones argon at the average simulation temperature, $T = 57.3$ K, the heat capacity determined from Eq. (6) was $C = 4.775 \times 10^5$ J/m^3 K. Interpolation of the experimentally obtained heat capacity [12] yielded $C = 8.897 \times 10^5$ J/m^3 K, which is of the same order of magnitude, but approximately twice the theoretical value. It is likely that this difference is due to the initial velocity estimate (Eq. (4)) being somewhat larger than the actual phonon speed of sound. Using these relationships to estimate the appropriate values for the argon variants provided a means of comparing KT with the simulation results for both homogenous and heterogeneous systems. Moreover, these relationships cannot and do not provide KT predictions of the simulation results. Additional theoretical tools, described in the next section, were also necessary to account for interfacial thermal resistance effects.

1.2. Existing interfacial thermal resistance theories

In the last half century, various experiments were conducted and theoretical models developed in attempts to explain thermal behavior at interfaces. The first measured interfacial resistance was reported by Kapitza [15] in 1941 while working with liquid helium. In 1952, Khalatnikov [16] presented a model attempting to explain that there is a "thermal boundary resistance" (TBR) at the boundaries of the helium that cause temperature discontinuities, or jumps. This model was a precursor to what is now known as the acoustic mismatch model (AMM). In 1955, Mazo and Onsager [17] presented the AMM nearly in its modern form, having done so independently of Khalatnikov's model. In 1959, Little [18] extended the AMM to handle solid–solid boundaries but found that creating solid–solid interfaces was experimentally difficult and results were hard to reproduce. In 1987, Swartz and Pohl [19] constructed a similar model called the diffuse mismatch model (DMM). Phelan [20] extended the DMM to handle calculation of the TBR for higher temperatures.

Both models attempt to describe how and why phonons are interrupted at interfaces. The AMM assumes that phonons are governed by continuum acoustics, i.e., they behave like plane waves. It also assumes that the interface between two dissimilar materials is treated as a perfect plane, and that the materials are treated as if they were a bulk medium. Thus, phonons impinging on the interface can reflect, refract and/or or mode-convert. An isotropic simplification is often made in calculating the phonon transmission probability in the AMM because phonons are affected by the mode of propagation (longitudinal or transverse), the angle of incidence, and the level of anisotropy in each material. The approximated transmission probability of phonons traveling from material 1 to material 2 is given by [21]

$$\alpha_{1\to 2} = \frac{4Z_1 Z_2}{(Z_1+Z_2)^2} \tag{9}$$

with

$$Z_i = \rho_i v_i \tag{10}$$

as the acoustic impedance, where ρ_i is the density of material i, and v_i is the corresponding mean phonon speed of sound. The full derivation of the thermal boundary resistance is beyond the scope of this paper; however, its final expression is given as [21]:

$$R_{B,AMM} = \left[\frac{\pi^2}{15}\frac{k_B^4}{\hbar^3}\left(\sum_j v_{1,j}^{-2}\Gamma_{1,j}\right)\right]^{-1} T^{-3} \tag{11}$$

where T is the temperature at the interface, and Γ is the transmission coefficient of the material of origin for mode of propagation j, which is defined as:

$$\Gamma_{1,j} = \int_{\theta=0}^{\pi/2} \alpha(\theta)_{1\to 2}\cos(\theta)\sin(\theta)\,d\theta \tag{12}$$

where θ is the angle of incidence. The DMM differs from the AMM mainly in the derivation of the transmission probability. While the AMM assumes specular interaction at a smooth interface, the DMM assumes diffuse scattering at a rough interface. For the molecular dynamics simulations performed for this study, all of the interfaces were considered "perfect", making application of the AMM theory most appropriate.

2. Molecular dynamics simulation method

The simulations in this study utilized non-physical Lennard–Jones materials so that a parametric investigation of the influence of interfacial effects on nanoscale thermal transport could be performed. Moreover, heterogeneous systems of thin films were modeled using a rectangular sim-

ulation cell with periodic boundary conditions (PBC) applied in the lateral dimensions only. While there are some drawbacks to using PBCs, such as periodicity effects and wave interference effects, their use has not been known to significantly affect equilibrium thermodynamics properties where interactions are relatively short ranged [4,22]. The Velocity-Verlet algorithm [23] was used to march the atoms through time. It is an extension to the standard Verlet method [24], which is accurate to the third order of the time step size and has minimal storage requirements. To provide acceleration data to the integration method, an all-pairs force calculation routine using neighbor lists was employed. The time step size used in each simulation was one femtosecond ($1\ \text{fs} = 10^{-15}$ s), which is consistent with other related studies [4,5,25,26]. The cut off distance in all cases was $r_c = 2.6\sigma$, using the largest σ value defined in the system.

To determine an effective thermal conductivity, a heat flux was imposed along the length of the lattice (x-axis), which was divided into five segments: two sets of stationary atoms, a cold bath, a warm bath, and a large, inner segment hosting regular atoms, as shown in Fig. 2a. The lattice dimensions used were $32a_0 \times 8a_0 \times 8a_0$, with $a_0 = 5.3$ Å, giving a total cell volume of 304 nm^3 which contained 8192 atoms. The regular atoms could include more than one type of material, depending on the simulation at hand. The stationary atoms were defined at each end of the cell as the four outer most planes and were used to keep thin films from melting or escaping into vacuum at the edges. Their positions and velocities were never updated, but their presence was considered during force calculations. The inner four planes adjacent to each set of stationary planes were defined as temperature baths. The bath planes on the left side represented the cold bath, while the bath planes on the right-side signified the warm bath. A constant quantity of energy was added to the warm bath and removed from the cold bath at each time step via momentum-conserving velocity rescaling [27]. By adding and removing the same amount of energy at each time step in the respective baths, a constant heat flux was induced across the thin film, all the while maintaining energy conservation. This method ensured a microcanonical constant-energy (NVE) ensemble.

To conduct the parametric study, argon's mass and bond strength, ε, were modified from 25% to 200% of their respective "true" values in increments of 25%. Systems were also created with σ-variants, however, early results indicated that σ was not an appropriate candidate for parameter modification since doing so (without additionally changing atomic spacing) drastically affected the behavior of the systems such that systems with large σ underwent compression, whereas the systems with small σ underwent expansion. This problem would have introduced unnecessary strain on the heterogeneous lattices. For any simulation involving two materials, Lorentz–Berthelot mixing rules were applied to the force and potential calculations [28].

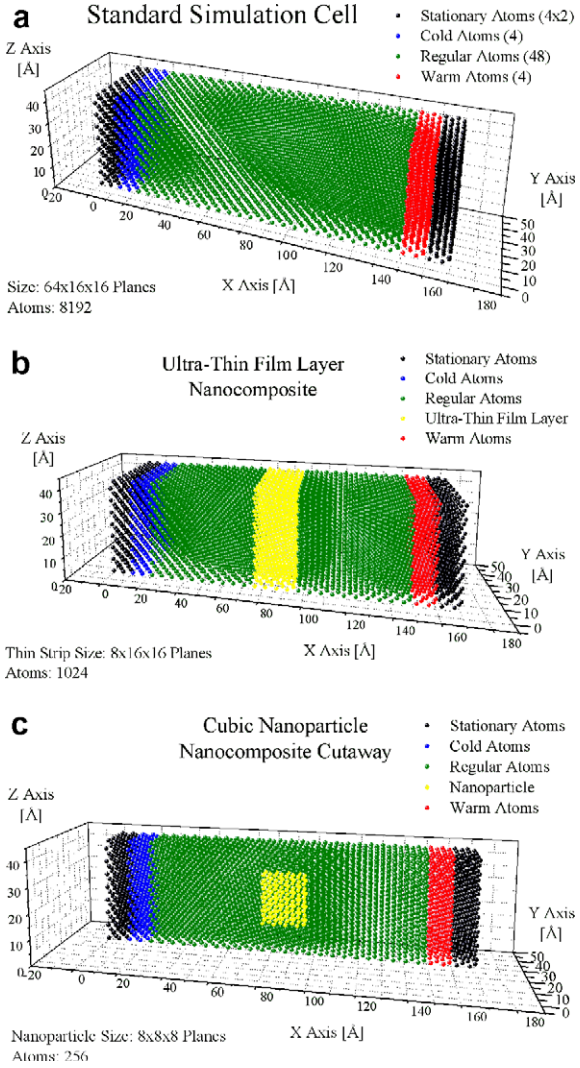

Fig. 2. A typical simulation cell is shown (a) with a three dimensional perspective. There are five logical segments: Left-side stationary atoms, cold temperature bath (left), regular atoms or argon matrix (middle), warm temperature bath (right), and right-side stationary atoms. A new layer of material is added to the middle of a typical simulation cell to create a layered thin film (b). A nanoparticle is added to the middle of a typical simulation cell to create a nanocomposite (c).

The initial simulations examined simple homogeneous thin films, while subsequent simulations modeled heterogeneous thin films of either layered films or "nanocomposites" comprised of cubic nanoparticles in an argon matrix. The configurations are illustrated in Fig. 2, with the lattice containing the cubic nanoparticle shown in a cutaway view. In the latter two cases, only the secondary material was subject to parameter modification. The lattice temperature observed throughout this study was 57.3 K, with an imposed temperature gradient of roughly 15 K. Large temperature gradients such as 15 K produce meaningful temperature data required for averaging, but care must be taken to ensure that the a change of state (e.g. from solid to fluid) does not arise along the length. Using information about the heat flux across the film, the

temperature gradient and the film thickness, an effective thermal conductivity was calculated using Fourier law. To account for propagation of error, the final average, variance, and standard error of these two properties were used to calculate the final effective thermal conductivity and its standard error for each simulation [4,22]. The maximum recorded statistical error in thermal conductivity for any one of the simulations presented herein was less than 2%.

3. Results and discussion

3.1. Argon variants

In order to analyze the results of the heterogeneous systems, benchmark thermal conductivity information for Lennard–Jones variant films comprised of only a single material was required. Each simulation was equilibrated for 1.0 million time steps before a minimum data collection period of 2.0 million time steps began. Equilibration was accomplished by first reaching equilibrium at the initial set temperature, $T = 60$ K, followed by the introduction of the heat flux, and finally ending after reaching a steady state. The steady-state average temperature of the *m*-variant and ε-variant systems was 57.3 K. To verify the applicability of Fourier law, temperature and heat flux profiles were plotted against the direction of heat flow to ensure linear temperature profiles and constant heat fluxes. Each of the simulations displayed these traits within reasonable tolerances, though, the heat flux profiles tended to be more scattered than temperature.

The thermal conductivity results from the argon mass variant films are shown in Fig. 3a. Note that each point represents one simulation's worth of data. Interestingly, the simulation results compared reasonably with kinetic theory as thermal conductivity decreased with increased mass; kinetic theory curves were generally lower than the simulation values but maintained a similar trend shape. The trend may be explained by understanding that atomic vibrational frequency is inversely proportional to mass, and using the harmonic approximation, frequency is inversely proportional to the square root of mass. Therefore, one would expect the exact behavior demonstrated in this figure by both curves. In Fig. 3b, ε was similarly varied, and an increase in thermal conductivity with increasing bond strength was exhibited. This was explained by understanding that an augmented bond strength (indicated by a deeper energy well as shown in Fig. 1) effectively results in an increased spring stiffness (see Eqs. (3) and (4)), and therefore a higher phonon velocity and thermal conductivity. It should be noted that in the 25% of ε_{Ar} simulation, the system collapsed (essentially melted) because the bond strength was so low the atoms could not maintain cohesion, hence the missing data point. Kinetic theory compared well with the simulation data for small percentages, but slowly fell away as either parameter was increased. There are several possibilities as to why both the mass and ε plots as compared with kinetic theory estimates differed. The most obvious reason concerns the definition of the phonon MFP. For both analyses the MFP was based on an experimental argon value. Compared to the "perfect" lattices simulated using MD, true bulk argon contains a large number of impurities and lattice defects which can significantly lower its thermal conductivity. Therefore, the MD simulated films should exhibit a higher MFP, and consequently, a higher thermal, as illustrated largely by Fig. 3a. However, there is no readily apparent explanation for why the data matched better at low parameter values. The overall difference between curves is likely a result of the harmonic-oscillation assumption used to produce the phonon velocity estimate in the kinetic theory analysis. Recall that by using that approximation, a higher velocity than the experimental value for pure argon was calculated. Moreover, after examining Eq. (2), an *upward* shift in the MD thermal conductivity curve (as compared with kinetic

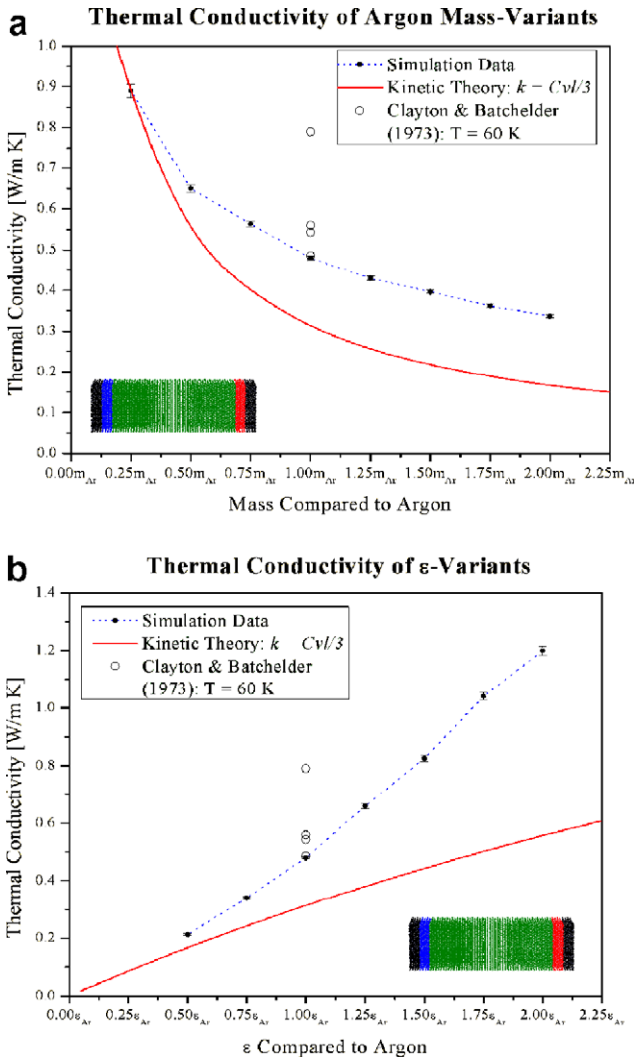

Fig. 3. Kinetic theory thermal conductivity, including Debye and harmonic-oscillation approximations, is compared to mass-variant simulation data (a) and to ε-variant simulation data (b). The dotted lines are presented merely as a guide to show the general trends of the thermal conductivity data. Four experimental data points are also shown for Ref. [29].

theory) might be expected as a result of this overestimation of velocity, but it is important to recognize that the velocity expression also affected the Debye calculation for heat capacity, C, which is directly proportional to the inverse of the third power of the phonon speed of sound. Therefore, an overestimate of the phonon velocity will actually yield a considerably smaller value for C, which would also result in the difference observed between the curves.

3.2. Layered thin films

Following the benchmark simulations of the individual argon variant films, heterogeneous thin films containing a single ultra-thin layer between two argon films were investigated. Again, the equilibration period lasted one million time steps and the data collection period lasted an additional minimum of two million time steps. The average system temperature still reached a steady-state temperature of $T = 57.3$ K.

For demonstration purposes, one representative temperature profile of the ultra-thin film systems from each of the mass and ε variations ($0.25m_{Ar}$ and $0.25\varepsilon_{Ar}$) are illustrated in Fig. 4. Note that each error bar represents the standard error of one simulation. The introduction of a secondary material into the argon matrix created a temperature profile exhibiting two distinct slopes – one corresponding to argon and the other to the variant material. As expected, a temperature jump occurred at each interface due to a thermal boundary resistance. The jump was less noticeable for decreased disparity, but was larger for the same percentage increase/decrease in mass than for ε. Since the temperature profiles are effectively nonlinear in these figures, Fourier law cannot be used in the conventional way to determine the thermal conductivity. Instead, Fourier law can be employed to calculate an "effective" thermal conductivity, which provides a means of comparison between the parametric combinations of layered systems. This value was determined from the total thickness of the system, the heat flux and the first and last planar temperatures of the regular atoms to provide an overall temperature gradient.

Fig. 5 shows that variation of m and ε produced similar trends in effective thermal conductivity. The curves indicated that there was a maximum thermal conductivity at (or near) the point representative of pure argon and as the disparity at the interfaces increased, the overall thermal conductivity of the system decreased. A slight deviation from this description occurred in the ε data where thermal conductivity peaked at a value for ε that was slightly higher than that of the pure argon film. This deviation can be explained through the combination of the following phenomena: As discussed previously for the case of an isolated film, an increase in the overall magnitude of ε prompted a general increase in thermal conductivity. However, the interfaces also played a role: with increased interfacial disparity, phonon scattering at the interfaces increased, which caused a reduction in effective thermal conductivity. Both m and ε trends initially exhibited similar slopes with the m curve showing near symmetry over the entire parametric range, but the ε trend trailed off less steeply after reaching a peak. Thus, interplay between the two phenomena caused the ε curve to peak at a value that was slightly higher than for pure argon and decrease at a slower rate than the mass curve for higher values. For moderate increases in ε, the ratio was seemingly less influential than influence of the larger ε material.

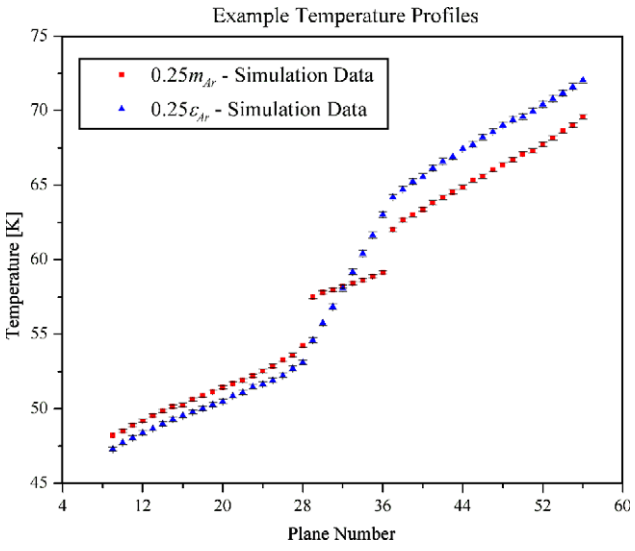

Fig. 4. Two representative temperature profiles, one each for $0.25m_{Ar}$ and $0.25\varepsilon_{Ar}$ modified materials, are shown. The ultra-thin layer exists between plane numbers 29 and 36.

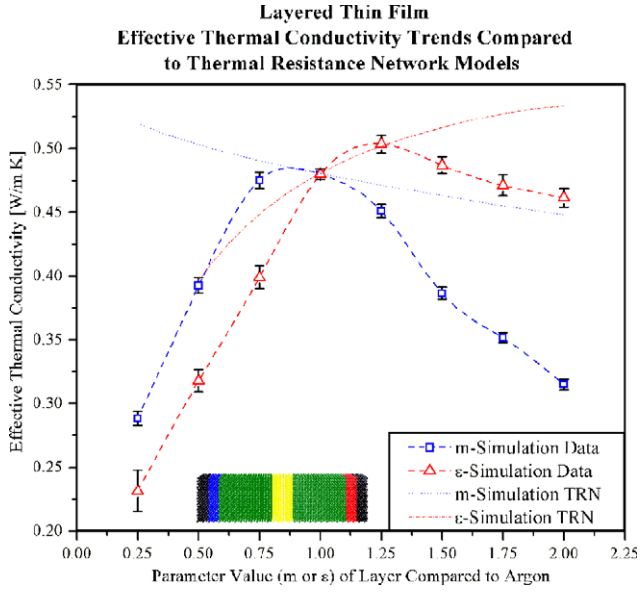

Fig. 5. The effective thermal conductivity trends of the layered thin films are shown in comparison with their respective thermal resistance network models. The lines are presented merely as a guide to show the general trends of the thermal conductivity data.

To fully appreciate the influence of the interfaces on thermal transport in the layered system, a thermal resistance network (TRN) of the thin films in series was employed to compare with MD results. The thermal resistance network consisted of three sections in series: a 20-plane wide argon matrix, followed by the 8-plane wide ultra-thin layer, and then another 20-plane wide argon matrix. Thermal boundary resistance was not included in the calculation of the TRN. "Bulk" thermal conductivities of the argon variant films (as generated from MD simulations) were used for the individual segment resistances. Note that k values obtained from simulations of isolated length-adjusted thin films were considered, rather than those of the "bulk" films, but did not present a realistic means for analyzing thermal boundary resistance. This is because an isolated film is confined by boundaries where total phonon reflection occurs, while a film adjacent to an interface will have some fraction of phonons reflected back into it, influencing thermal transport within the film itself. The use of bulk simulated values provided a better upper limit on k for the TRN comparison with the data. Using the method outlined by Choi [25], the $32a_0$ length chosen for the simulations yields a bulk thermal conductivity for argon just 6% less than when $L \to \infty$. In addition to the effective thermal conductivity curves produced by the MD simulations, Fig. 5 also shows their respective TRN counterparts. In both cases, because the TRN ignored interfacial resistances, it consistently produced thermal conductivities that were higher than the simulation values. For pure argon, however, it predicts the correct value since no interface existed. The effect was exacerbated as the disparity was increased because of increased phonon scattering at the interfaces.

While a comparison of the data to the TRN provides a good initial insight to the effects of the interfaces, that insight can be furthered by using the AMM to compare the theoretically calculated thermal boundary resistance (TBR) to one derived from the simulation data. The AMM value for each variant was calculated from Eq. (11), using the corresponding mass and phonon velocity (Eq. (4) where mass, ε, and σ are required for the calculation). The assumptions made when calculating R_B using the AMM values were that (1) the Lennard–Jones velocity estimate (Eq. (4)) could be used in place of the average speed of sound; (2) this value could also be used to represent both the longitudinal and transverse speeds of sound; and (3) α was not a function of phonon angle of incidence θ, which set $\Gamma = \alpha/2$. The thermal boundary resistance from the simulation data was obtained from using the ratio of the magnitudes of the temperature jump at each interfaces, ΔT, and the heat flux, Q (e.g. $\Delta T/Q$). Fig. 6 illustrates the comparisons between the TBR from the MD simulations and the AMM calculations. To simplify the comparison, the left- and right-side interface resistances were plotted as a sum. The AMM produced relatively high thermal resistance values for low mass (Fig. 6a) and low ε (Fig. 6b) values. Moreover, with an increase in mass or ε, the thermal resistances decreased. The simulation data displayed a similar decreasing trend for low values, but after the point of no disparity, the thermal resistances showed an increase. Note that for the MD simulation results with respect to ε, a slight decrease appears at 200% of ε_{Ar}. However, it should be mentioned that the temperature jumps between the two adjacent planes at the interface obtained from the simulation data did not apparently capture the full effects of interfacial resistance. Rather, it seemed that the effects were spread across several planes, and therefore using data for ΔT from only two adjacent places would obviously lead to some degree of error for the comparison. Even with the discrepancies between the AMM and simulation data, the comparisons for the mid-range parameter disparities were remarkably good, indicating that the AMM theory provides a decent explanation of the effects of interfacial thermal resistance for a "perfect" lattice if the acoustic impedance mismatch is not severe.

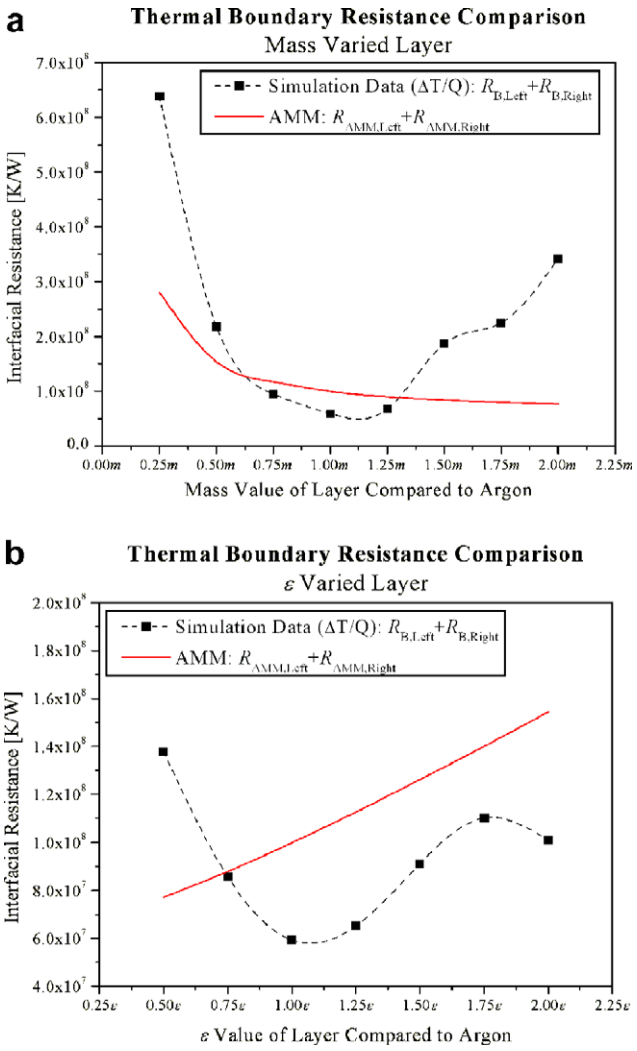

Fig. 6. The sum of the left- and right-side thermal resistances from the simulation data is compared against the summed AMM thermal boundary resistances for both mass and ε. The dashed lines are presented merely as a guide to show the general trends of the thermal conductivity data.

3.3. Cubic nanoparticle embedded in an argon matrix

The layered film provided important information of the influence of the interface on thermal transport, and while these films are prevalent structures in a variety of systems, composites of particles embedded in a matrix are also quite common. It naturally follows that replacing the ultra-thin film with a cubic nanoparticle will provide further insight into how interfacial thermal resistance effects thermal transport. Since periodic boundary conditions were imposed in the lateral directions, the cell in which a single nanoparticle resides was repeated in the y- and z-directions infinitely, thereby forming a so-called "nanocomposite" thin film with infinite nanoparticles. For the MD simulations, the same size simulation cell, atom count, initial temperature, and equilibration and data collection periods were implemented as discussed previously. The nanoparticle was eight planes thick, similar to the ultra-thin film, but then chopped down to eight planes laterally.

The temperature profiles obtained from the simulations for the nanocomposite system were similar in nature to the layered films, however, they did not show as large of a temperature jump at the nanoparticle boundaries. Fig. 7 compares the effective thermal conductivities of the nanocomposite with the layered system discussed previously as mass and ε are varied, respectively. The results demonstrate that for the case of the nanocomposite, variation of both mass and ε led to a much less pronounced reduction in thermal conductivity. As illustrated by the curves, the decrease in interfacial area of the nanocomposite from the layered system limits the influence of the interfaces on the nanocomposite as a whole; fewer phonon reflections occur because there is physically less of a disturbance in their path across the film and the reduction in thermal conductivity is less pronounced. Nonetheless, the trends demonstrate that as the disparity at the interface increased, the overall thermal conductivity of the nanocomposite decreased with a peak at (or near) the point representative of pure argon. Similar to the case of the layered film, the ε curve indicated an offset of that peak towards higher values of bond strength. At large values of ε, the nanocomposite showed a similar competition between the increased disparity wanting to cause a reduction in effective thermal conductivity and the higher thermal conductivity of the nanoparticle itself. However, the effective thermal conductivities for both cases were practically equal at $1.75\varepsilon_{Ar}$ and $2.00\varepsilon_{Ar}$. This was likely a result of the fact that while the nanoparticle itself possesses a large thermal conductivity at these values, it comprises a smaller fraction of the total simulation cell than the ultra-thin film.

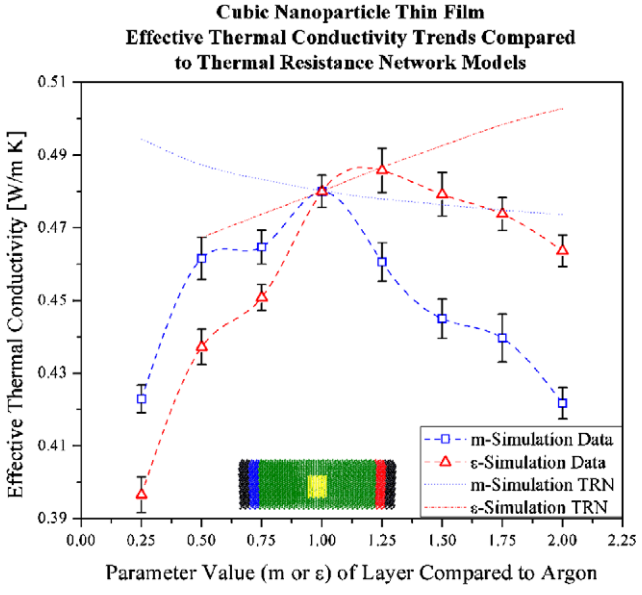

Fig. 7. The effective thermal conductivity trends of the cubic nanoparticle embedded nanocomposites are shown in comparison with their respective thermal resistance network models. The lines are presented merely as a guide to show the general trends of the thermal conductivity data.

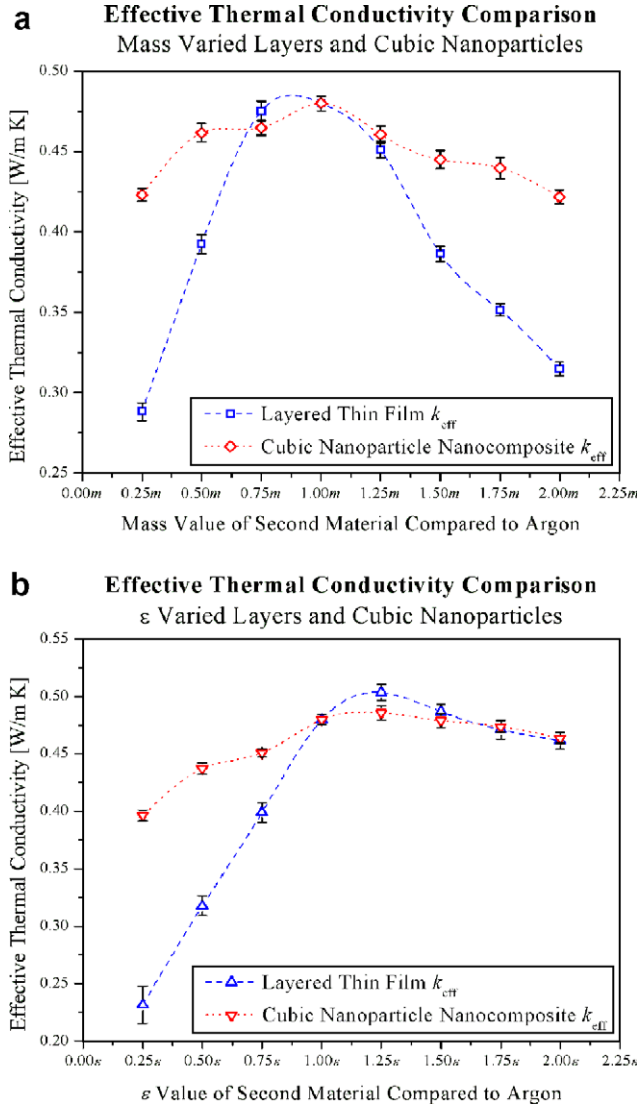

Fig. 8. Comparisons of the effective thermal conductivity trends between the layered thin films and cubic nanoparticle embedded nanocomposites are shown. The lines are presented merely as a guide to show the general trends of the thermal conductivity data.

The nanocomposite system was also compared with a thermal resistance network to help elucidate the role of the interface. It should be noted that for the layered system, there were two interfaces to consider, but with the presence of a cubic nanoparticle a total of six interfaces exist, of which only two were normal to the flow of heat. Therefore, a more complex network of series and parallel resistances was constructed for the comparison. As shown in Fig. 7, the TRN demonstrated that the interface played a large role in influencing a reduction in effective thermal conductivity with increased disparity. However, the decrease occurred to a lesser extent than for the case of the layered films. Again, this is likely a result of phonons finding a less resistive path where the interface was not present.

Finally, the results of the ultra-thin layered films were compared to those of the nanocomposite films. Fig. 8a and b illustrates both mass curves and both ε curves, respectively. In the case of the mass results, interfacial area appears to dominate the extent to which thermal conductivity is affected. The ε results are more interesting in that the layered films experience a significantly larger drop in thermal conductivity for smaller values of ε but experience nearly the same thermal conductivities for ε greater than that of pure argon. This perhaps implies that variation of mass may produce more influential interfaces, increased phonon reflection.

4. Summary and conclusions

Molecular dynamics was used to study the influence that interfaces have on nanoscale thermal transport in solid argon and argon-based variants. To accomplish this, the mass m and bond strength ε of pure argon were systematically modified to create variations on two types of heterogeneous systems: a layered film and a nanocomposite film. A comparison of thermal conductivity was made between simulation results and kinetic theory as well as thermal resistance network models and the acoustic mismatch model to help provide a basic understanding for analysis of the heterogeneous systems. Application of harmonic-oscillation and Debye approximations with KT yielded thermal conductivities that were on the same order of magnitude as the MD results. Generally speaking, kinetic theory produced trend curves and the simulation data followed each other fairly well, comparing better with lower parameter values yet falling away slightly for higher parameter values. The differences were most likely due to the assumptions made in approximation the mean free path, phonon velocity, and heat capacity. The use of an experimental mean free path in the theoretical calculations that was likely lower than the true mean free path of the simulated materials undoubtedly contributed to the disagreement. Moreover, the known overestimation of the phonon velocity corresponding to pure argon likely indicated that the variant velocity estimates were also high. Not only did this affect the calculation of thermal conductivity directly, but heat capacity was also affected since it depends on velocity. To truly appreciate the deviation from kinetic theory type behavior, additional coding to capture the simulated heat capacity and phonon velocities of each simulation is necessary, and will be the focus of future work.

The introduction of a second material into an argon film generally decreased its overall thermal conductivity. However, an exception was observed where slightly increased ε values produced a slight increase in thermal conductivity over pure argon. A comparison of the layered system with the nanocomposite demonstrated that the presence of a nanoparticle was less influential in reducing thermal conductivity than the thin layer. This behavior was expected since the phonons had less of an obstruction along the path of heat flow. Application of the thermal resistance network without the AMM illustrated the significance of the interfacial effects as it predicted thermal conductivity values whose offset increased with greater interfacial disparity. Comparison of calculated AMM values to the simulated interfacial resistances showed promise; however, the AMM did not fully capture the behavior observed in the simulations. This may be due to several factors including the aforementioned assumptions used to predict phonon velocities which significantly affect the calculation of interfacial resistances, as well as the techniques used to collect and analyze the simulation data. In all, the results indicate that combining a TRN with the AMM to describe nanocomposite thin films provides a means for investigating interfacial thermal resistance effects. More importantly, the results show that the configuration studied can be used to study more complex structures with reasonable success. Continuation of this work will involve improvements to the MD simulator, as well as the investigation of new systems that may exhibit interesting interfacial thermal effects. Moreover, the simulator will be expanded to collect the data necessary for calculation of dispersion relations, phonon velocities and heat capacities.

References

[1] D.G. Cahill, W.K. Ford, K.E. Goodson, G.D. Mahan, A. Majumdar, H.J. Maris, R. Merlin, S.R. Phillpot, Nanoscale thermal transport, J. Appl. Phys. 93 (2) (2003) 793–818.
[2] S.G. Volz, J.B. Saulnier, M. Lallemand, B. Perrin, P. Depondt, M. Mareschal, Transient Fourier-law deviation by molecular dynamics in solid argon, Phys. Rev. B 54 (1) (1996) 340–347.
[3] S. Berber, Y.K. Kwon, D. Tománek, Unusually high thermal conductivity of carbon nanotubes, Phys. Rev. Lett. 84 (20) (2000) 4613–4616.
[4] J.R. Lukes, D.Y. Li, X.G. Liang, C.L. Tien, Molecular dynamics study of solid thin-film thermal conductivity, Trans. ASME 122 (2000) 536–543.
[5] A.R. Abramson, C.L. Tien, A. Majumdar, Interface and strain effects on the thermal conductivity of heterostructures: a molecular dynamics study, J. Heat Transfer 124 (2002) 963–970.
[6] P. Keblinski, S.R. Phillpot, S.U.S. Choi, J.A. Eastman, Mechanisms of heat flow in suspensions of nano-sized particles (nanofluids), Int. J. Heat Mass Transfer 45 (2002) 855–863.
[7] A.J.H. McGaughey, M. Kaviany, Thermal conductivity decomposition and analysis using molecular dynamics simulations. Part I.

Lennard–Jones argon, Int. J. Heat Transfer Mass Transfer 47 (2004) 1783–1798.
[8] A.J.H. McGaughey, M. Kaviany, Thermal conductivity decomposition and analysis using molecular dynamics simulations. Part II. Complex silica structures, Int. J. Heat Transfer Mass Transfer 47 (2004) 1799–1816.
[9] S.G. Volz, J.B. Saulnier, G. Chen, P. Beauchamp, Computation of thermal conductivity of Si/Ge superlattices by molecular dynamics techniques, Microelectron. J. 31 (2000) 815–819.
[10] R.J. Stevens, P.M. Norris, L.V. Zhigilei, Molecular-dynamics study of thermal boundary resistance: evidence of strong inelastic scattering transport channels, ASME International Mechanical Engineering Congress and Exposition, Anaheim, CA, 2004.
[11] G.J. Keeler, D.N. Batchelder, Measurement of the elastic constants of argon from 3 to 77 K, J. Phys. C, Solid State Phys. 3 (1970) 510–522.
[12] E.R. Dobbs, G.O. Jones, Theory and properties of solid argon, Rep. Prog. Phys. 20 (1957) 516–564.
[13] C. Kittel, Introduction to Solid State Physics, seventh ed., John Wiley & Sons, USA, 1996.
[14] N.W. Ashcroft, N.D. Mermin, Solid State Physics, Saunders College Publishing, USA, 1976.
[15] P.L. Kapitza, The study of heat transfer in helium II, J. Phys. 4 (1941) 181–210.
[16] I.M. Khalatnikov, J. Exp. Theor. Phys. USSR 22 (1952) 687–704.
[17] R.M. Mazo, Theoretical Studies on Low Temperature Phenomena, Ph.D. Thesis, Yale University, New Haven CT, 1955.
[18] W.A. Little, The transport of heat between dissimilar solids temperatures, Canadian J. Phys. 37 (1959) 334–349.
[19] E.T. Swartz, R.O. Pohl, Thermal resistances at interfaces, Appl. Phys. Lett. 51 (26) (1987) 2200–2202.
[20] P.E. Phelan, Application of diffuse mismatch theory to the prediction of thermal boundary resistance in thin-film high-T_C superconductors, J. Heat Transfer 120 (1998) 37–43.
[21] E.T. Swartz, R.O. Pohl, Thermal boundary resistance, Rev. Mod. Phys. 61 (3) (1989) 605–668.
[22] M.P. Allen, D.J. Tildesley, Computer Simulation of Liquids, Oxford University Press, New York, 1987.
[23] W.C. Swope, H.C. Anderson, P.H. Berens, K.R. Wilson, A computer simulation method for the calculation of equilibrium constants for the formation of physical clusters of molecules: application to small water clusters, J. Chem. Phys. 76 (1982) 637–649.
[24] L. Verlet, Computer 'experiments' on classical fluids. I. Thermodynamical properties of Lennard–Jones molecules, Phys. Rev. 159 (1) (1967) 98–103.
[25] S.H. Choi, S. Maruyama, K.K. Kim, J.H. Lee, Evaluation of the phonon mean free path in thin films by using classical molecular dynamics, J. Korean Phys. Soc. 43 (5) (2003) 747–753.
[26] S.H. Choi, S. Maruyama, Variations in the thermal conductivity of insulating thin films with temperature and pressure, J. Korean Phys. Soc. 45 (4) (2004) 897–906.
[27] B. Hafskjold, T. Ikeshoji, Partial specific quantities computed by nonequilibrium molecular dynamics, Fluid Phase Equilib. 104 (1995) 173–184.
[28] R.C. Reid, J.M. Prausnitz, B.E. Poling, The Properties of Gases and Liquids, Mc-Graw Hill, New York, NY, 1987.
[29] F. Clayton, D.N. Batchelder, Temperature and volume dependence of the thermal conductivity of solid argon, J. Phys. C: Solid State Phys. 6 (1973) 1213–1228.